Exchange Biased Magnetic Nanostructures

Kai Liu[1,2], J. Nogués[3], C. Leighton[4], Ivan K. Schuller[2], S. M. Baker[5], M. Tuominen[6], T. P. Russell[7], H. Masuda[8], and K. Nishio[8]

[1]*Department of Physics, University of California, Davis, CA 95616, USA*
[2]*Department of Physics, University of California - San Diego, La Jolla, CA 92093, USA*
[3]*Institució Catalana de Recerca i Estudis Avaçats (ICREA) and Departament de Física, Universitat Autònoma de Barcelona, 08193 Bellaterra, Spain*
[4]*Dept. of Chemical Engineering and Materials Science, Univ. of Minnesota, MN 55455, USA*
[5]*Department of Chemistry, Harvey Mudd College, Claremont, CA 91711, USA*
[6]*Physics Department, University of Massachusetts, Amherst, MA 01003, USA*
[7]*Polymer Science and Engineering, University of Massachusetts, Amherst, MA 01003, USA*
[8]*Applied Chemistry Dept., Tokyo Metropolitan Univ., Hachioji, Tokyo 192-0397, Japan*

Abstract

We have investigated the exchange bias phenomenon in nanostructured ferromagnet / antiferromagnet (FM/AF) bilayers to probe the roles of domain size and domain morphology. By using a diblock copolymer nanolithography technique and separately a nanoporous alumina shadow mask method, we have achieved ultrafine nanostructures, as small as 20 nm, over macroscopic areas (1 cm^2). We have observed an enhancement of the exchange bias in patterned structures over that in uniform thin films. We have also found a pronounced asymmetry in magnetic hysteresis loops that vanishes at the FeF_2 Néel temperature. The asymmetry is due to different magnetization reversal mechanisms that are intrinsic to both exchange bias and the nanostructure. We also show that exchange bias may be used as an additional and tunable means of anisotropy to stabilize magnetization in nanomagnets. By placing the FM dot arrays on top of an AF layer, we have observed improved thermal stability in terms of the magnetic hysteresis loop squareness.

I. Introduction

The exchange bias phenomenon in ferromagnet/antiferromagnet (FM/AF) bilayers has attracted a great deal of interest due to its elusive mechanism and important applications [1-4]. Normally, the magnetic hysteresis loop of a single FM layer is centered about zero-field. However, when an FM layer is exchange-coupled to an AF layer, by cooling in a field across the AF Néel temperature T_N, it exhibits a shifted loop with an enhanced loop width. This phenomenon allows one to pin, and thus manipulate, the magnetization direction of the FM, which is highly desirable for device applications such as spin-valve type devices.

Although the exact mechanism of exchange bias remains unclear, it is generally believed that magnetic domains, particularly AF domains, are crucial [5-11]. Different domain models with domain wall perpendicular or parallel to the interface have been proposed [5,6,10,11]. One direct method to probe these domains and the roles of domain sizes is to investigate exchange biased nanostructures with feature sizes smaller than the characteristic magnetic domain sizes (~1□m for FM and smaller for AF). However, the ease of fabrication and characterization of such nanostructures often scales inversely with the physical dimension. Furthermore, the small volumes of the FM nanostructures associated with the small sizes also adversely affect their thermal stability.

In this work, we report the synthesis of exchange-biased nanostructures over macroscopic areas (1 cm^2) using a diblock copolymer nanolithography method and separately a nanoporous alumina shadow mask technique. We have found an enhanced exchange bias due to the reduced sample lateral dimension, along with pronounced magnetization reversal asymmetry. Additionally, we have observed evidence of improved thermal stability in exchange-biased FM nanodots.

II. Experimental Procedures

For sample preparation, we have used 1cm x 1cm single crystal MgO (100) substrates, and Fe as the FM layer and FeF_2 as the AF layer (which has a Néel temperature of 80 K). Two different techniques have been used to achieve FM/AF exchange biased nanostructures. In the first approach, a diblock copolymer nanolithography has been used to realize a nanoporous Fe-network structure on top of a uniform FeF_2 layer. A schematic of the sample synthesis process is shown in Figure 1a. Thin films of Fe (15 nm)/FeF_2 (20 nm) were first deposited by e-beam evaporation, capped with a 4 nm Al layer. A diblock copolymer layer of polystyrene and polymethyl-methacrylate, denoted PS-*b*-PMMA, is then spin-coated on top of the film. The two blocks of the copolymer are chemically distinct and spontaneously self-assemble into microdomains upon annealing [12, 13]. The microdomain morphology can be tuned by using different volume ratios of the two polymer types. In our experiment, the minor component, PMMA, forms an array of 20 nm size cylinders. Under ultraviolet exposure and sonication the PMMA blocks are degraded and removed, while the PS blocks are crosslinked and immobilized. This produces a nanoporous template that is subsequently used to transfer the pattern into the underlying film by ion milling. By stopping the ion milling at the interface of Fe/FeF_2, we have fabricated a network of Fe on top of a uniform FeF_2 layer, as seen in the atomic force microscopy image shown in Figure 1c [14]. The dark and bright areas are, respectively, the pores and the cross-linked network. The transfer of the template to the film was excellent. The characteristic dimensions of the network, the pore size and pore separation, are both about 20 nm.

In the second approach, an alumina shadow mask technique has been used to achieve nanomagnet arrays with magnet size of about 60 nm over a 1 cm^2 area [15]. A schematic of the sample preparation process is shown in Figure 1b. A thin porous aluminum oxide

membrane (~300 nm) is first created by an anodic oxidation and etching process [16, 17]. It is then transferred onto a substrate [18, 19] and used as a shadow mask during a subsequent e-beam evaporation of a 15 nm thick Fe layer. Portions of the deposition flux goes through the holes and deposit onto the substrate, whereas the rest is blocked by the membrane. A liftoff of the membrane then leaves behind only the nanodots, as shown in Figure 1d. In the alumina mask, the pores are fairly uniform in size, with an average diameter of 61 ± 5 nm. In the Fe nanodots, the size, along with the narrow size distribution, is well maintained through the liftoff process. The average diameter of the dot is 59 ± 6 nm. Indeed the combination of a thin mask and a directional flux during the e-beam evaporation minimized any "shadowing" effect that could have compromised the structural integrity. For comparison and consistency, three samples have been made on the same substrate as described elsewhere [15]: 1). 60 nm-size Fe-nanodots (15 nm thick) / MgO; 2). 60 nm-size Fe-nanodots (15 nm) / FeF_2 (90 nm) /MgO, and 3). Fe-film (15 nm) / MgO. The exact growth conditions have been reported in earlier studies [14, 20]. The Fe layer thus prepared is polycrystalline, and grows similarly on MgO and FeF_2. The AF FeF_2 grows as twinned quasi-epitaxial layer along the compensated (110) surface (twin domain size ~10 nm) [21].

The macroscopic areas of both types of nanostructures allow convenient magnetic characterizations by superconducting quantum interefrence device (SQUID) magnetometry.

III. Results and Discussions

Exchange Bias

Effects of domain sizes on the exchange bias have been studied in the nanoporous network structure prepared by the diblock copolymer technique (Figure 1a & 1c). Magnetic hysteresis loops of the patterned network samples as well as uniform thin films of Fe and Fe/FeF_2 are shown in Figure 2. In simpler cases of a single 15 nm thick Fe network and a uniform Fe film, the hysteresis loops are qualitatively the same in the temperature range studied (10-300 K). However, the magnetization reversal is sharper and the coercivity is smaller in the network sample, as shown in Figure 2a and 2b. This is due to the reduced anisotropy in the network geometry as the physical dimensions approach zero. The behaviors of Fe/FeF_2 bilayers, however, are drastically different in the network and uniform film geometries. Figure 2c and 2d show the hysteresis loops of a uniform film of Fe/FeF_2 and a Fe-network / uniform-FeF_2 taken at 10 K, respectively, field-cooled in 5 kOe from room temperature. The uniform Fe/FeF_2 film shows a symmetric hysteresis loop, shifted by an exchange field of H_E = -200 Oe. In contrast, in Fe-network / uniform-FeF_2, the loop has a pronounced asymmetry, with sharper switching and a larger loop shift. The switching from positive to negative saturation is rather abrupt. Upon returning, the magnetization reversal first gradually proceeds to about –160 Oe, at which point it quickly switches to positive saturation. The exchange field is about -260 Oe. The temperature dependence of exchange field is shown in Figure 3. In the uniform Fe/FeF_2, the exchange field shows a plateau before vanishing at the FeF_2 T_N of 80 K. In the Fe-network /uniform-FeF_2 the exchange field is larger and follows a similar temperature dependence.

To monitor the unusual switching characteristics, we define the switching width as the field change needed to switch between ±70 % saturation magnetization M_S. Figure 4a shows the temperature dependence of the switching width in the network geometry. In the decreasing-field branch, the width is essentially flat, within a narrow range of 50-80 Oe. In the increasing-field branch, the width stays around 210 Oe until 50 K, beyond which it precipitously drops and eventually overlaps with the decreasing-field branch at 80 K and above. The difference between the two switching widths, or the loop asymmetry, is shown in Figure 4b as a function of temperature. The fact that the asymmetry vanishes at the AF Néel temperature indicates its exchange bias origin. In comparison, in uniform FeF_2/Fe films, the switching width is about 300 Oe in both branches at 10-100 K (Figure 4c) and the asymmetry

is no more than 60 Oe (Figure 4d). This indicates that the pronounced asymmetry observed in the networks is not only due to the exchange bias between FeF_2 and Fe, but also intrinsic to the network nanostructure. Likely different magnetization reversal mechanisms are involved in decreasing- and increasing-field branches of the loop.

To determine the reversal mechanisms of the network sample at the two branches of the loop, we have performed the following reversibility tests from saturation. For the decreasing / increasing field branch, the sample was brought from positive / negative saturation to every field value along the branch, then back to the exchange field to measure the remanence. It is observed that only the initial gradual reversal process from negative saturation is reversible, while the sharp switching processes are irreversible. This is also confirmed by minor loop measurements along different locations of the major loop. These results indicate that the reversal from negative saturation initiates by coherent rotation. Along other parts of the hysteresis loop, the reversal likely involves both domain wall motion and incoherent rotation processes that cannot be distinguished by the reversibility test. This is also confirmed by anisotropic magnetoresistance measurements [14].

The interesting loop asymmetry and the larger H_E observed in the network sample are intimately related to its nanostructure. Earlier neutron scattering [22] and transport measurements [23] indicated that in an exchange biased system the magnetization reversal mechanism can be different along decreasing and increasing field branches of the loop. The decreasing-field side of the loop occurs by domain rotation (Stoner-Wohlfarth), whereas the increasing-field side is by domain wall motion. As shown in Figure 2d, this affects drastically the behavior of the Fe film; in the decreasing-field branch of the loop the change is small whereas on the increasing-field side the magnetization remains almost constant and then suddenly the magnetization jumps. The behavior on increasing-field side is consistent with a domain wall mechanism which is pinned in the pores. Since the reversal mode in the decreasing-field side is due to domain rotation, the pores have no effect. Many interesting question arise in this context which are presently under investigation, such as the lateral size and vertical etching depth dependence of exchange bias, effects of patterning on magnetic anisotropy, thermal stability, nanopatterning processes, etc.

The observed larger exchange field in the patterned structures is consistent with a random field model proposed by Li and Zhang [11]. Their model emphasizes the role of FM domain size, determined by the competition between FM-FM exchange and the random field due to the interfacial FM-AF interactions. When the FM-FM interaction is strong, as favored by smaller AF grain size or thicker FM layer, the FM forms larger domains (>> AF grain size) and the net random field averages out to be small, thus smaller H_E and H_C. It is clear from this model that limiting the lateral dimension of the AF/FM bilayer alone is not expected to alter exchange bias significantly until the dimensions are below the FM domain (typically on the micron scale) or AF grain size (usually much smaller) in uniform films. In the present network geometry, the nanoporous Fe network effectively reduces the FM-FM interactions, thus favoring the formation of smaller FM domains, larger net random fields, and larger exchange field. A larger exchange field in nanostructured AF/FM bilayers has also been observed recently in CoO/NiFe system [24]. Ultimately, as the replication of the porous network goes deeper into the bilayer and the dimensions of the AF/FM entities become smaller and smaller, the exchange field is limited by superparamagnetism.

B. Thermal Stability

For the Fe nanodot arrays made by the alumina shadow mask technique (Figure 1d), we have investigated their thermal stability in the aforementioned three samples. At 300 K, the uniform Fe film exhibits the usual square loop with a small coercivity H_C of 25 Oe, as shown

in Figure 5. The squareness of the loop, defined as the ratio of remnant magnetization M_R over saturation magnetization M_S, is 84 %. In contrast, the loop of the Fe nanodot arrays at 300 K is much more sheared with a larger H_C of 110 Oe and a smaller squareness of 15 %. Primary contributions to the different loop shapes are the demagnetization field and, to a lesser degree, magnetic dipolar interactions between the dots. Because of the polycrystalline nature of the Fe film and nanodots, contributions from magnetocrystalline anisotropy are negligible. The increased coercivity in Fe nanodots is a well-known phenomenon for fine magnetic particles [25]. The small dimensions of the dots impede the formation of multi-domains and the magnetization reversal proceeds primarily through rotation. The small remnant magnetization of the Fe nanodots is an indication of the reduced anisotropy energy relative to the thermal fluctuations, given that the simultaneously made Fe nanodots and film on the same substrate should have similar structural characteristics. The anisotropy energy (product of anisotropy constant K and volume V) decreases as the nanodot becomes smaller, and the effects of thermal fluctuation become significant, eventually leading to superparamagnetism. Therefore the remnant magnetization or squareness of the loop may be used as an indication of the thermal stability of the nanomagnets.

The exchange anisotropy in FM/AF system is an *external* source for magnetization stabilization. For the sample with Fe nanodot arrays on top of a FeF_2 layer, the exchange anisotropy was introduced by field cooling the bilayer in a 5 kOe field from 300 K to below the FeF_2 T_N (~80 K). A resultant hysteresis loop at 10 K is shown in Figure 6, shifted from zero field by 31 Oe. With increasing temperature, the exchange field H_E eventually vanishes at around 80 K, the FeF_2 T_N, as shown in Figure 6 inset. Notice that the magnitude of H_E is one order of magnitude smaller than that in uniform Fe/FeF_2 bilayer films [14, 20]. This is due to the exposed FeF_2 surface during the alumina mask application process, resulting in contaminated Fe/FeF_2 interface. It further attests to the interfacial nature of EB.

Even with the modest exchange bias, the remnant magnetization M_R and squareness of the hysteresis loop are improved. For example, at 10 K, M_R is 64 % of M_S at the exchange field of –31 Oe, while at zero field the magnetization is 67 % and 61 % of M_S in the decreasing- and increasing-field branches, respectively (Figure 6). In comparison, the unbiased Fe nanodots grown on the same substrate show a M_R of 52 % M_S (Figure 6). We can estimate the exchange anisotropy energy per unit area at 10 K as $H_E tM$=0.077 erg/cm^2, where t is the Fe layer thickness. Over the 60nm size area of a nanodot, the anisotropy is about 1.35 eV, or about 50 times the thermal energy at room temperature. Additionally, EB can be controlled by a variety of parameters, such as constituent material, deposition order, cooling field strength, interface roughness, crystallinity, etc., which can be used as additional degrees of freedom to control the magnetization stabilization.

IV. Conclusion

In summary, we have realized exchange bias nanostructures over macroscopic areas using a diblock copolymer technique as well as an alumina shadow mask technique. Nanostructures with feature sizes as small as 20 nm have been realized over macroscopic areas (1 cm^2). We have observed an enhancement of the exchange bias in patterned structures over that in uniform thin films. We have also found a pronounced asymmetry in magnetic hysteresis loops that vanishes at the FeF_2 Néel temperature. The asymmetry is due to different magnetization reversal mechanisms that are intrinsic to both exchange bias and the nanostructure. We also show that exchange bias may be used as an additional and tunable means of anisotropy to stabilize magnetization in nanomagnets.

This work has been supported by US-DOE, US-AFOSR, UC Davis-FRG, and Catalan DGR.

References

W. H. Meiklejohn and C. P. Bean, Phys. Rev. 102, 1413 (1956).
B. Dieny, V. S. Speriosu, S. S. P. Parkin, B. A. Gurney, D. R. Whilhoit, and D. Mauri, Phys. Rev. B 43, 1297 (1991).
For a recent review, see e.g., J. Nogués and I. K. Schuller, J. Magn. Magn. Mater. 192, 203 (1998).
A. E. Berkowitz and K. Takano, J. Magn. Magn. Mater. 200, 552 (1999).
D. Mauri, H. C. Siegman, P. S. Bagus and E. Kay, J. Appl. Phys. 62, 3047(1987).
A. P. Malozemoff, J. Appl. Phys. 63, 3874 (1988).
N. C. Koon, Phys. Rev. Lett. 78, 4865 (1997).
M. D. Stiles and R. D. McMichael, Phys. Rev. B 59, 3722 (1999).
T. C. Schulthess and W. H. Butler, Phys. Rev. Lett. 81, 4516 (1998).
M. Kiwi, J. Mejía-Lopez, R. D. Portugal, and R. Ramirez, Appl. Phys. Lett. 75, 3995 (1999).
Zhanjie Li and Shufeng Zhang, Phys, Rev. B 61, 14897 (2000); Appl. Phys. Lett. 77, 423 (2000).
M. Park, C. Harrison, P. Chaikin, R. A. Register, and D. H. Adamson, Science, 276, 1401 (1997).
E. Huang, L. Rockford, T. P. Russell, and C. J. Hawker, Nature, 395, 757 (1998).
Kai Liu, Shenda M. Baker, Mark Tuominen, Thomas P. Russell, and Ivan K. Schuller, Phys. Rev. B 63, 060403(R) (2001).
Kai Liu, J. Nogués, C. Leighton, I. V. Roshchin, H. Masuda, K. Nishio, and I. K. Schuller, Appl. Phys. Lett. submitted.
F. Keller, M. S. Hunter, and D. L. Robinson, J. Electrochem. Soc. 100, 411 (1953).
G. E. Thompson, R. C. Furneaux, G. C. Wood, J. A. Richardson, and J. S. Gode, Nature 272, 433 (1978).
H. Masuda, K. Nishio, and N. Baba, Thin Solid Films 223, 1 (1993).
H. Masuda and K. Fukuda, Science 268, 1466 (1995).
J. Nogués, D. Lederman, T. J. Moran, and I. K. Schuller, Phys. Rev. Lett., 76, 4624 (1996).
M. R. Fitzsimmons, C. Leighton, J. Nogués, A. Hoffmann, Kai Liu, I. K. Schuller, C. F. Majkrzak, J. A. Dura, J. R. Groves, R. W. Springer, P. N. Arendt, V. Leiner, and H. Lauter, Phys. Rev. B 65, 134436 (2002).
M. R. Fitzsimmons P. Yashar, C. Leighton, Ivan K. Schuller, J. Nogués, C. F. Majkrzak, and J. A. Dura, Phys. Rev. Lett. 84, 3986 (2000).
C. Leighton, M. Song, J. Nogués, M. C. Cyrille, and I. K. Schuller, J. Appl. Phys. 88 344 (2000).
L. Sun, Y. Ding, C. L. Chien, P. C. Searson, Phys. Rev. B 64 184430 (2001).
B. D. Cullity, *Introduction To Magnetic Materials*, M. Cohen, Ed. (Addison-Wesley Publishing Company, Inc., 1972).

Figure Captions

Figure 1. Schematics of (a) a diblock copolymer nanolithography technique for creating a nanoporous network and (b) an alumina shadow mask technique for creating arrays of nanodots. (c) is an atomic force microscopy phase image of a porous Fe (15nm thick) network. The dark and bright areas are pores and networks, respectively. (d) is a scanning electron microscopy image of arrays of Fe nanodots made by the shadow mask technique.

Figure 2. Magnetic hysteresis loops of (a) a uniform single Fe layer (15 nm thick), (b) an Fe-network (15 nm) film, (c) a uniform Fe (15 nm) / FeF_2 (20 nm) film, and (d) a Fe-network (15 nm) / uniform-FeF_2 (20 nm) film at 10K, after field cooling in 5 kOe from 300 K.

Figure 3. Temperature dependence of exchange field H_E in uniform Fe/FeF_2 film (solid symbols) and Fe-network/uniform-FeF_2 (open symbols), after field cooling in 5 kOe from 300 K.

Figure 4. Temperature dependence of magnetization switching width between ±70 % M_S for (a) Fe-network/uniform-FeF_2 and (c) uniform Fe/FeF_2 film. The difference between the two branches, or the loop asymmetry, is shown in (b) and (d) for the two samples. Solid lines are guides to the eye.

Figure 5. Magnetic hysteresis loops of a uniform Fe film (15 nm thick) and arrays of Fe nanodots (60 nm wide, 15 nm thick) at 300 K.

Figure 6. Magnetic hysteresis loops of Fe nanodot arrays (60 nm wide, 15 nm thick) on MgO (unbiased, open symbols) and a 90 nm-thick FeF_2 film (exchange biased, solid symbols) at 10 K, after field cooling in 5 kOe from 300 K. The inset shows the temperature dependence of the exchange field for the biased Fe nanodots.

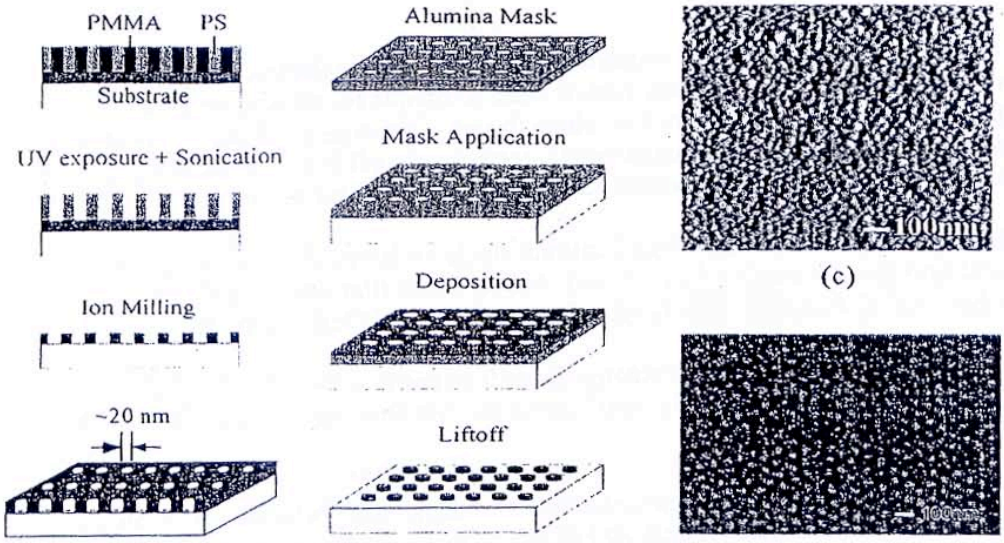

Figure 1

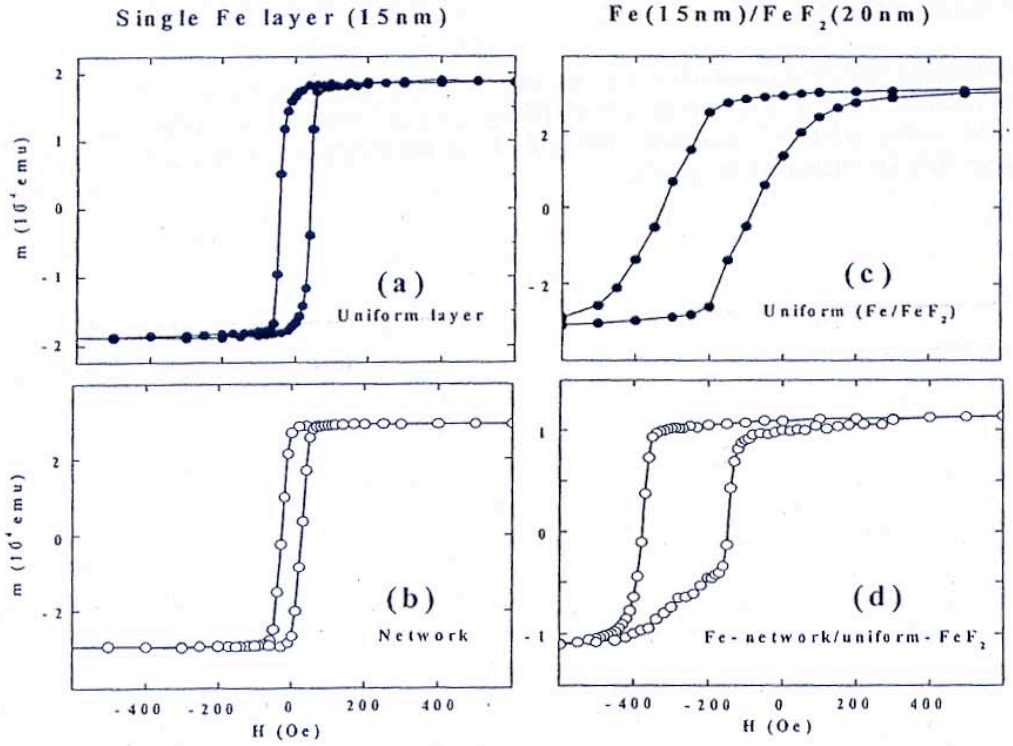

Figure 2

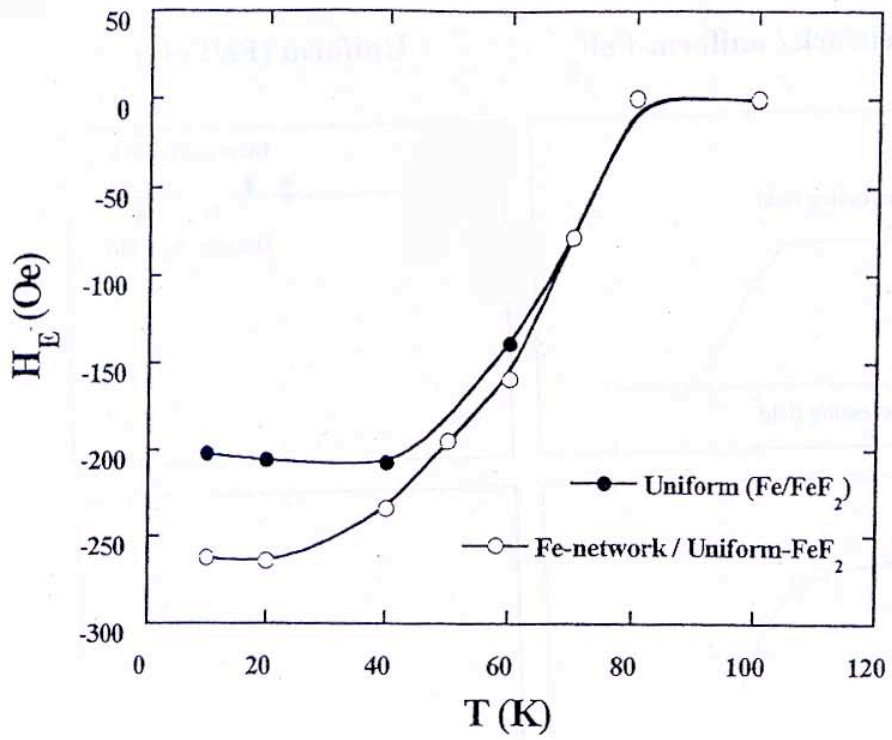
50
0
-50
-100
-150
-200
-250
-300
H_E (Oe)
0
20
40
60
80
100
120
T (K)
Uniform (Fe/FeF$_2$)
Fe-network / Uniform-FeF$_2$

Figure 3

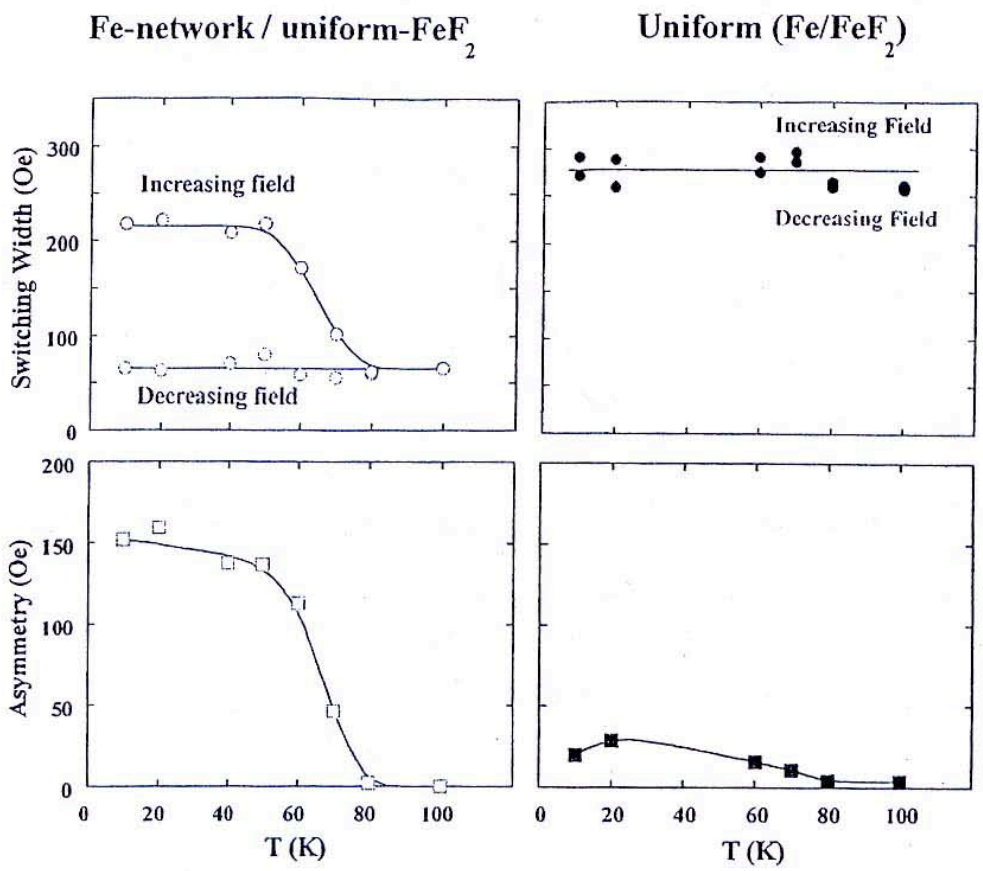
Fe-network / uniform-FeF2
Uniform (Fe/FeF2)
Switching Width (Oe)
Increasing field
Decreasing field
Increasing Field
Decreasing Field
Asymmetry (Oe)
T (K)
T (K)

Figure 4

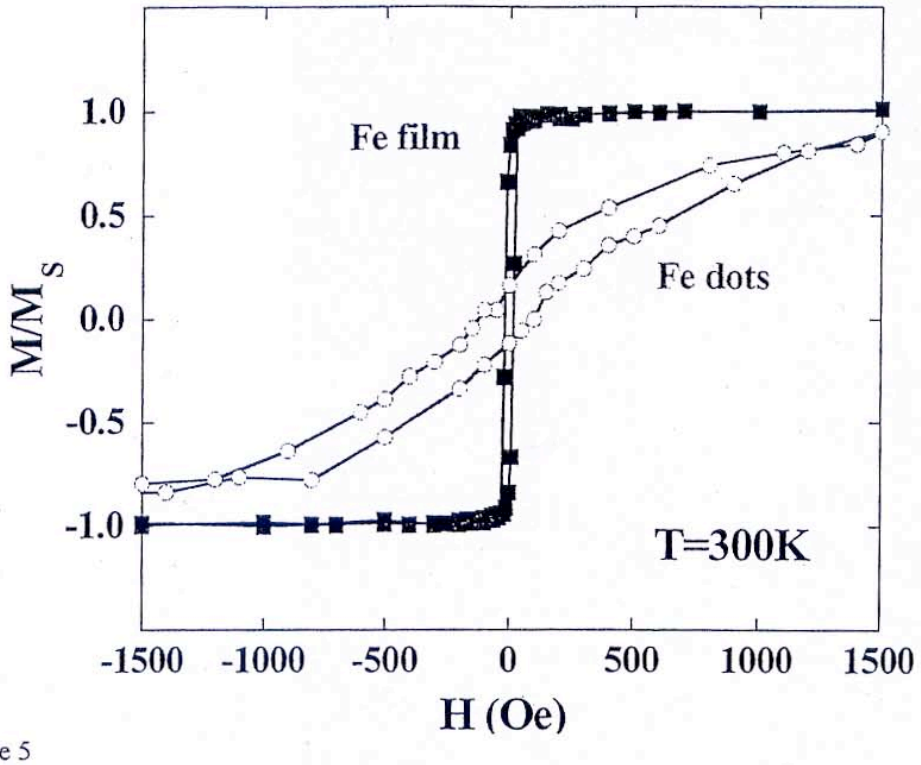
1.0
0.5
0.0
-0.5
-1.0
M/M_S
Fe film
Fe dots
T=300K
-1500
-1000
-500
0
500
1000
1500
H (Oe)

Figure 5